Investigations of complete and incomplete fusion in $^{12}C+^{93}Nb$ and $^{16}O+^{89}Y$ by recoil range measurements

B. S. Tomar, A. Goswami, A. V. R. Reddy, S. K. Das, P. P. Burte, and S. B. Manohar
Radiochemistry Division, Bhabha Atomic Research Centre, Bombay 400 085, India

Bency John
Nuclear Physics Division, Bhabha Atomic Research Centre, Bombay 400 085, India
(Received 19 May 1993)

The recoil range distribution of the radioactive evaporation residues in the reaction of 63 and 77.5 MeV ^{12}C with ^{93}Nb and that of 68 MeV ^{16}O with ^{89}Y have been measured using the recoil catcher technique followed by gamma spectrometry. The linear momentum transfers inferred from these recoil range distributions were used to identify the evaporation residues formed by complete and incomplete fusion mechanisms. The data are compared with Monte Carlo simulation of recoil range distributions of products formed by complete fusion to extract the contribution of incomplete fusion in the individual channels. The observations are discussed in the framework of existing models.

PACS number(s): 25.70.Gh, 25.70.Jj

INTRODUCTION

Heavy ion reactions with projectile energies close to Coulomb barrier are dominated by compound nucleus (CN) and direct reactions. As the projectile energy is increased, compound nucleus formation is hindered and incomplete fusion (ICF) starts competing with complete fusion (CF). In ICF reactions, only a part of the projectile fuses with the target. A common feature of these reactions is the observation of light ejectiles at forward angles with approximately beam velocity. This type of ICF reaction is commonly observed with low-Z heavy ions as the projectile [1]. These reactions were first observed by Britt and Quinton [2] and Galin *et al.* [3]. Particle-gamma coincidence studies by Inamura *et al.* [4] contributed a great deal to the understanding of the mechanism of ICF reactions. Such reactions are difficult to explain in terms of deep inelastic collisions as the mass flow is always from the projectile to target.

Several models are used to explain these ICF reactions, namely, breakup fusion [5], sum rule model [6], promptly emitted particles (PEP's) [7], exciton model [8], etc. In the sum rule model of Wilczynski *et al.* [6], ICF is viewed as arising from peripheral collisions in the range of angular momenta just above the critical angular momentum (l_{cr}) for complete fusion. Udagawa and Tamura [5] explained ICF in terms of the breakup of the projectile followed by fusion of one of the fragments with the target. According to the PEP model [7], the particles transferred from the projectile to target may get accelerated in the nuclear force field of the target and thereby acquire extra velocity to escape. The exciton model [8] assumes that the projectile nucleons undergo a series of collisions with target nucleons creating particle-hole excitations which deexcite by emitting fast particles. All these models have been used to fit the experimental data obtained using projectile energies above 10 MeV/nucleon. Some recent studies, however, showed the onset of ICF just above the Coulomb barrier. Parker, Hogan, and Asher [9] observed forward peaked alpha particles in reaction of 6 MeV/nucleon low-Z heavy ions on ^{51}V. Morgenstern *et al.* [10] observed ICF components in the velocity spectra of evaporation residues (ER's) in a reaction of ^{40}Ar with boron and carbon targets. Tserruya *et al.* [11] found evidence for ICF from time-of-flight measurements of ER's in a reaction of 5.5–10 MeV/nucleon ^{12}C with ^{120}Sn, ^{160}Gd, and ^{197}Au.

The two important aspects which need to be addressed are (i) whether these ICF reactions are governed by entrance channel mass asymmetry or the property of the composite nucleus and (ii) angular momenta involved in these reactions. Morgenstern *et al.* [12] showed that, for different reactions at the same relative velocity, ICF is more likely for a mass asymmetric entrance channel than that for a mass symmetric one. Recent studies by Vineyard *et al.* [13] and Beck *et al.* [14] support the systematics proposed by Morgenstern *et al.* [12]. The sum rule model predicts that ICF is confined to the angular momenta above the critical angular momentum (l_{cr}) for complete fusion of the projectile and target. The peripheral nature of ICF reactions has also been emphasized by Trautmann *et al.* [15]. On the other hand, some recent studies indicate the involvement of central collisions in ICF, particularly in the case of spherical targets [16].

Recently [17], we measured the excitation functions for ER's in $^{12}C+^{93}Nb$ and $^{16}O+^{89}Y$ systems with projectile energies in the range of 4–6.5 MeV/nucleon. Both reactions lead to the formation of same compound nucleus ^{105}Ag. We observed that the alpha emission products $^{99,100}Rh$ in both systems have much higher cross sections than those predicted by the CF process. Further, the two alpha emission products, namely, $^{96,95}Tc$ in $^{12}C+^{93}Nb$, showed a much higher cross section than that in $^{16}O+^{89}Y$ at the same excitation energy of the CN. We attributed these observations to the occurrence of ICF involving the breakup of the projectile ^{12}C (^{16}O)

into $\alpha+^{8}$Be ($\alpha+^{12}$C) followed by fusion of either of the two fragments with the target ^{93}Nb (^{89}Y) giving Rh and Tc products in ^{12}C+^{93}Nb system and Rh and Nb products in the ^{16}O+^{89}Y system, respectively. Similar results were also obtained by Parker, Hogan, and Asher [18] in a similar system, namely, ^{20}Ne+^{93}Nb. They measured the cross sections and recoil range distributions of the radioactive products as well as the emitted particle spectra at beam energies of 106 and 148 MeV and observed significant contributions of ICF to the various reaction products.

Differential recoil range measurements provide information about the linear momentum transfer in a reaction [19–21] and have been very useful in understanding the mechanism of noncompound nucleus reactions. In this paper, we present the results of our measurements of the recoil range distribution (RRD) of the various radioactive products formed in the 63 and 77.5 MeV ^{12}C+^{93}Nb and 68 MeV ^{16}O+^{89}Y reactions. The recoil ranges measured in this work are projected ranges along the beam direction and do not reveal any angular dependence of cross sections and velocities of the evaporation residues. In order to identify the yields associated with CF and ICF, the observed recoil range distributions are compared with those predicted by Monte Carlo simulation of CF and ICF processes. Cross sections for CF and ICF for individual channels are established. The results are discussed in terms of the existing models of the ICF reactions.

EXPERIMENTAL PROCEDURE

The experiments were carried out at the BARC-TIFR Pelletron accelerator at Bombay. Thin targets of metallic niobium and yttrium of thickness around 100 μg/cm^2 were prepared by vacuum evaporation onto thin aluminum foils of thickness 100 μg/cm^2. A stream of 15 aluminum catcher foils having a thickness of around 100 μ g/cm^2, prepared by the same technique, was used to stop the recoiling products. The thicknesses of the targets and aluminum foils were measured, with an accuracy of <5%, by determining the energy loss suffered by the 5.49 MeV alpha particles from an ^{241}Am source while traversing through it. The stopping power table of Northcliffe and Schilling [22] was used to determine the thickness from the energy loss measurements. In the irradiation assembly, the target was mounted with the aluminum backing facing the beam. The target was bombarded with the projectile for about 12 h. The beam current, measured with an electron suppressed Faraday cup placed behind the target catcher assembly, was about 50 nA (particle). After the irradiation, the activities of individual reaction products were measured by following the gamma activities in the individual catcher foils for a period of 10 days. The measured activities were corrected for their decay to obtain the activities at the end of irradiation [$A(T_i)$]. The cross sections (σ) for a particular product in different foils were obtained using the equation

$$\sigma = A(T_i)/[N\phi\varepsilon I\{1-\exp(-\lambda T_i)\}], \quad (1)$$

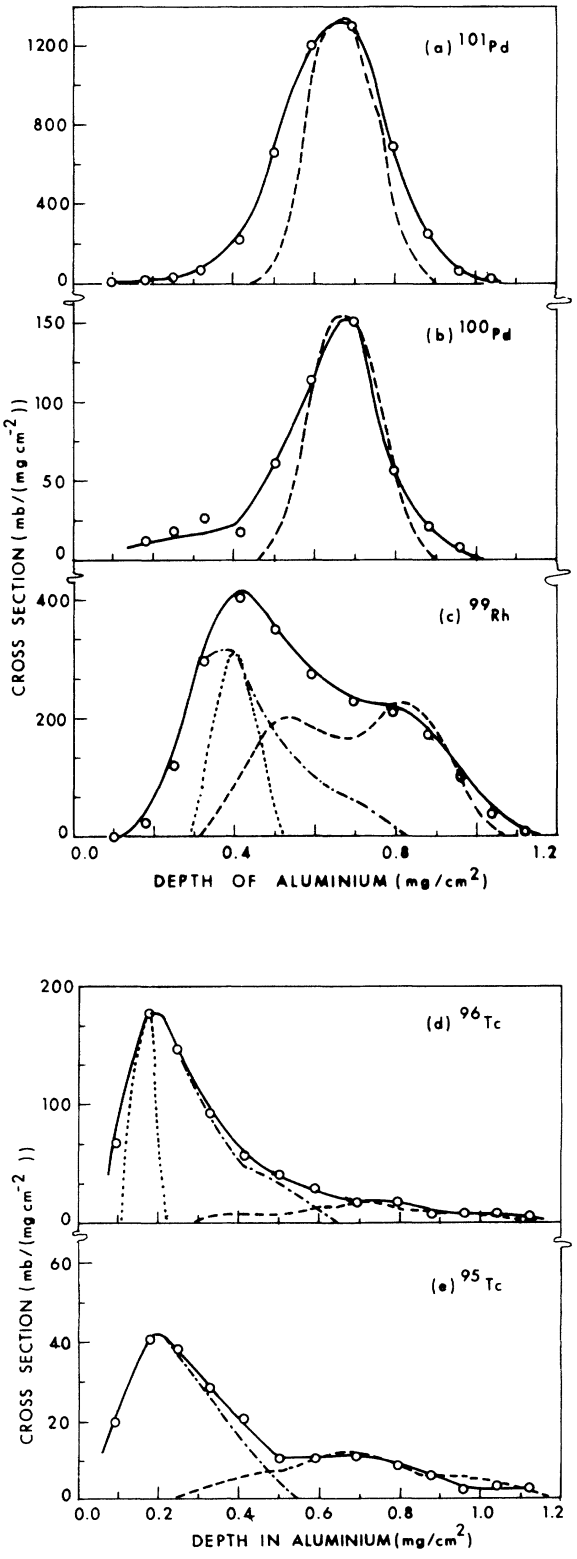

FIG. 1. Recoil range distributions in 63 MeV ^{12}C+^{93}Nb. The solid lines are guides to the experimental data. Dashed lines are the PACE2 curves for the CF process. The dotted lines are obtained by simulation of the ICF process based on the breakup fusion model. The dash-dotted curves are the ICF components obtained by subtracting the CF part from the experimental curves.

where N is the number of target atoms per cm^2, ϕ is the beam intensity, ε is the detector efficiency, I is the branching ratio of the gamma ray of the product, and λ is its decay constant. The nuclear spectroscopic data used in the present work have been given in Ref. [17]. The measured cross section of a particular product in each foil was divided by its thickness and plotted against the cumulative catcher thickness to obtain the RRD. As there was no attempt to obtain the absolute cross sections in this measurement, the distributions were normalized to the absolute cross sections measured previously [17].

ANALYSIS OF EXPERIMENTAL DATA

The RRD's for the various reaction products, studied in the present work, are shown in Figs. 1, 2, and 3 for 63 and 77.5 MeV ^{12}C and 68 MeV ^{16}O induced reactions, respectively. The solid lines are guides to the experimental points. The abscissa in the figures represents the range projected along the beam axis. The error on the cross section data is of the order of 10–15 %, which is primarily due to the counting statistics.

The RRD's for the ER's formed by CF were simulated using the Monte Carlo simulation code PACE2 [23]. The level density parameter was taken as $A/8$ MeV^{-1}. The average gamma transition probabilities were taken from the compilation of Endt [24]. Other input parameters were used as default values recommended for this mass region. This code gives the double differential cross section ($d^2\sigma/dE\,d\Omega_{\rm lab}$) for ER's, which was transformed into the projected range distribution along the beam axis using the range energy table of Northcliffe and Schilling [22]. The RRD's obtained using the PACE2 code were normalized to the experimental RRD's by adjusting the height and keeping the peak position and the width as constant. The RRD's for different reaction channels, predicted by PACE2, are shown as dashed curves in the re-

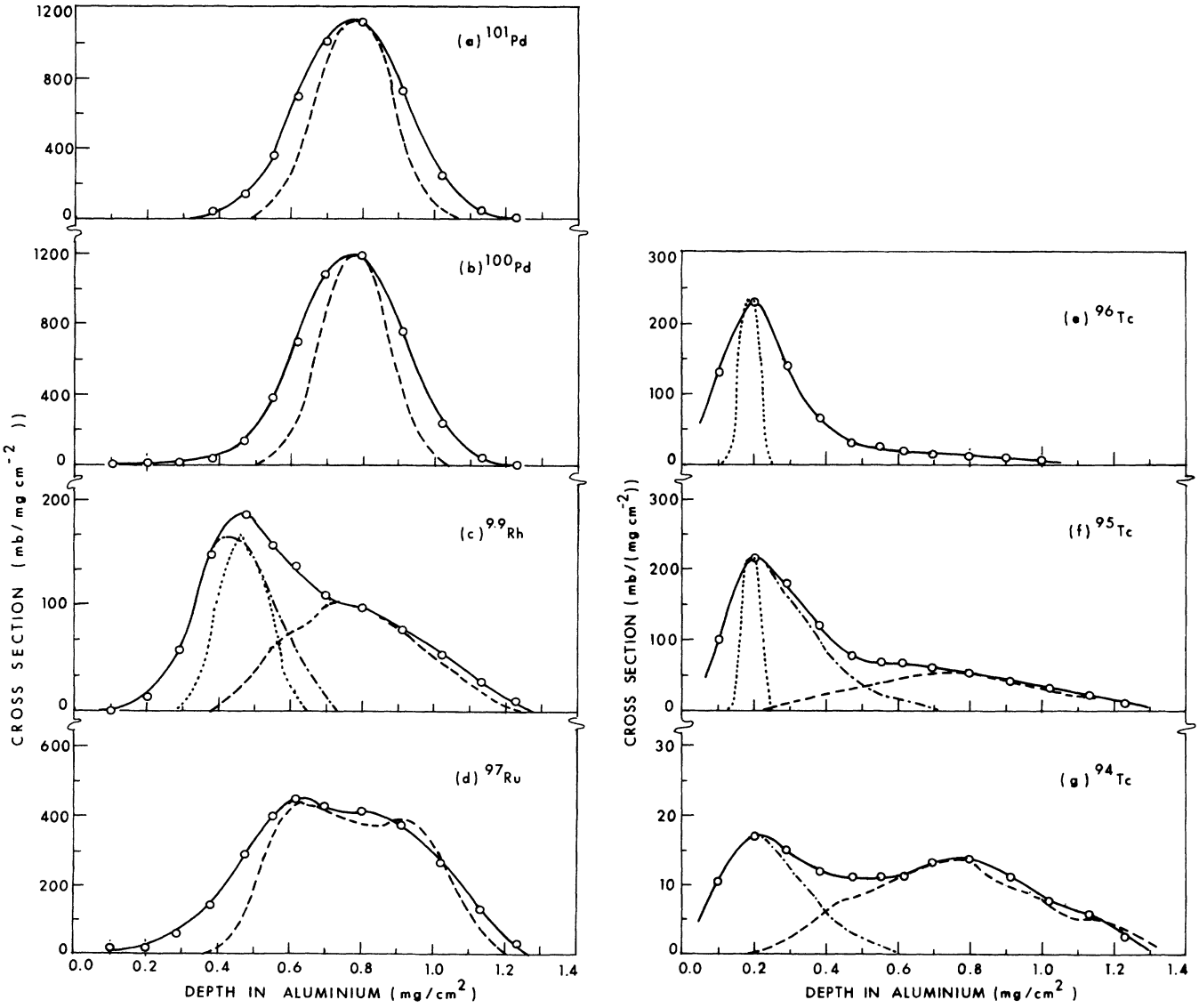

FIG. 2. Recoil range distributions in 77.5 MeV ^{12}C+^{93}Nb. The notation is the same as in Fig. 1.

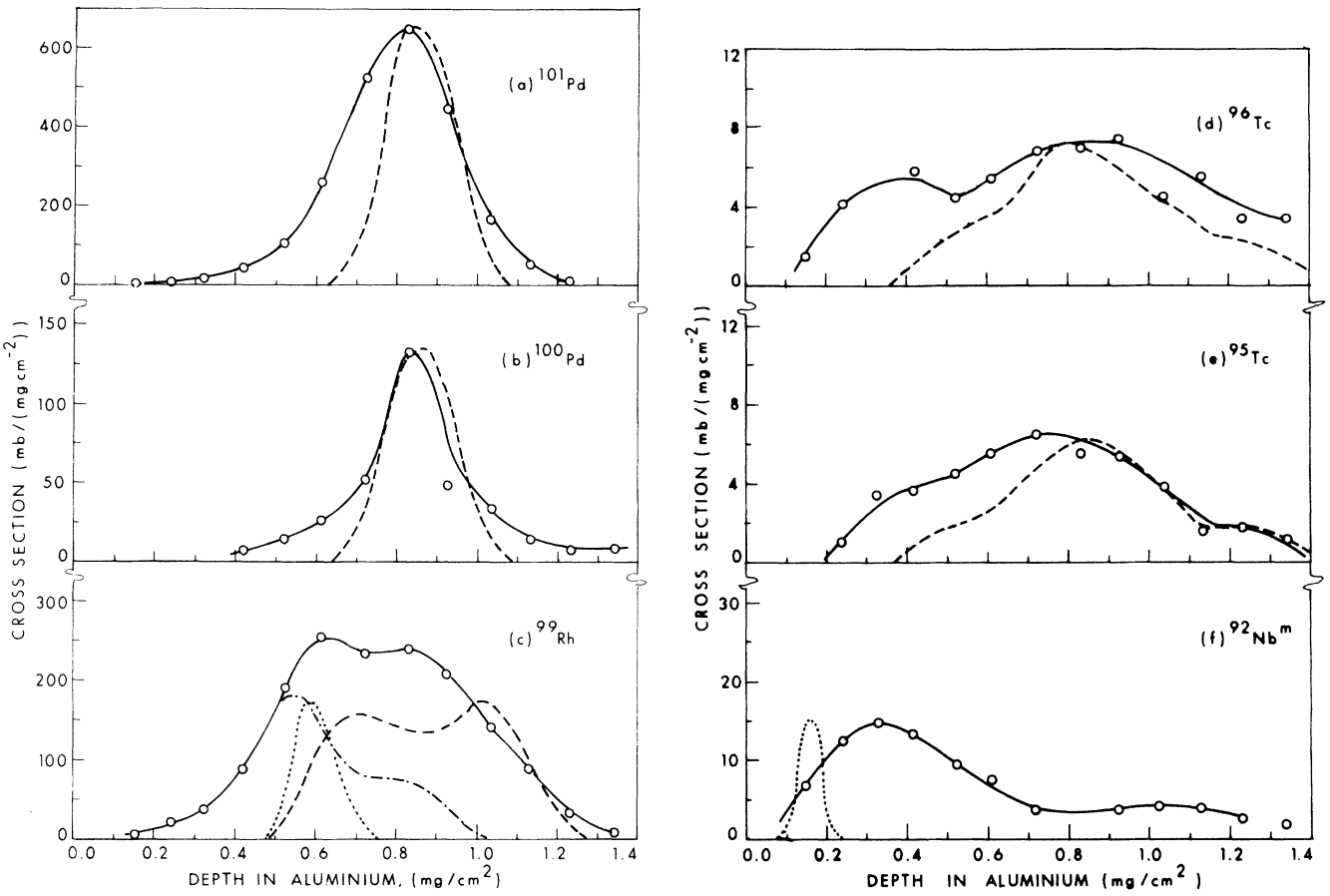

FIG. 3. Recoil range distributions in 68 MeV ^{16}O+^{89}Y. The notation is the same as in Fig. 1.

spective figures. A comparison between the excitation functions obtained using the PACE2 and CASCADE (used in Ref. [17]) codes by using identical input parameters showed that the data are in overall agreement within 30% except in the case of silver isotopes where the difference was as large as a factor of 2. However, it was seen that the changes in the level density parameters and gamma transition probabilities do not significantly affect the RRD's.

Table I shows the mean ranges, for the CF and ICF components, obtained by fitting of the experimental RRD's either into a single Gaussian (in case of ER's formed only by CF) or into two Gaussians (for ER's formed by both CF and ICF). Also shown are the mean ranges obtained from the PACE2 curves. The errors shown on the mean ranges are the least squares fitting errors. The actual errors are about 5%, which result mainly from the error in thickness measurement.

The RRD's for ^{101}Pd and ^{100}Pd are shown in Figs. 1(a), 2(a), and 3(a) and 1(b), 2(b), and 3(b), respectively. It is seen that the experimental curves agree well with the PACE2 curves, except for the large width. The small shifts in the case of ^{16}O+^{89}Y may reflect the error in measurement of the thickness of the catcher foils. This shows that the palladium products are solely produced following the complete fusion of projectile and target.

The RRD for ^{99}Rh ($\alpha 2n$ channel), obtained by summing the data for ^{99}Rh^{m} and ^{99}Rh^{g}, deviates markedly from the prediction of the PACE2 code in all the three cases as seen in Figs. 1(c), 2(c), and 3(c). The two peaks in the PACE2 curve [Figs. 1(c) and 3(c)] are due to the alpha particles emitted at forward and backward angles in the center-of-mass system. In the case of 77.5 MeV ^{12}C [Fig. 2(c)], the two-peak structure is smeared owing to interference from the $2p4n$ channel. The experimental curves show a low range component and a shoulder on the higher range side. Except for the double-peak structure, the shoulder agrees with the PACE2 curve and hence can be identified as arising from the CF process. The ICF component was obtained by subtracting the CF component from the experimental curve and is shown as dash-dotted curve in the respective figures. The mean ranges corresponding to CF and ICF are shown in Table I. The RRD for ^{97}Ru ($\alpha p3n$ channel) could be obtained only in the ^{12}C+^{93}Nb system at $E_{\rm lab}$ = 77.5 MeV and is shown in Fig. 2(d). The PACE2 curve in the figure was obtained by adding the distributions for the isobars ^{97}Rh and ^{97}Ru as the experimental data represent the cumulative cross section of ^{97}Ru. The experimental data agree well with the PACE2 curve showing its formation only by CF processes.

The data for technetium isotopes ($2\alpha xn$ channels) in the ^{12}C+^{93}Nb system show a dominant low range component due to ICF while the CF part appears as a long range tail as shown in Figs. 1(d), 1(e), and 2(e)–2(g).

TABLE I. Mean ranges for evaporation residues.

	63 MeV $^{12}C+^{93}Nb$			77.5 MeV $^{12}C+^{93}Nb$			68 MeV $^{16}O+^{89}Y$		
Nuclide	ICF	CF	PACE	ICF	CF	PACE	ICF	CF	PACE
^{101}Pd		0.650 ±0.001	0.673		0.768 ±0.001	0.777		0.804 ±0.003	0.861
^{100}Pd		0.650 ±0.010	0.673		0.767 ±0.001	0.775		0.823 ±0.013	0.861
^{99}Rh	0.412 ±0.008	0.733 ±0.025	0.531[a] 0.821	0.449 ±0.004	0.748 ±0.034	0.755	0.584 ±0.016	0.884 ±0.022	0.715[a] 1.027
^{97}Ru					0.731 ±0.012	0.775			
^{96}Tc	0.201 ±0.016		0.639	0.204 ±0.009		0.74		0.76 ±0.05	0.834
$^{95}Tc^{g}$	0.218 ±0.008		0.645	0.226 ±0.005		0.74		0.729 ±0.018	0.836
$^{94}Tc^{g}$				0.213 ±0.008		0.74			
$^{92}Nb^{m}$							0.366 ±0.014		

[a]The two values represent two peaks of the PACE curve.

The PACE2 code reproduces the tail part of the distribution. The ICF component was extracted by subtracting the PACE2 curve from the experimental curve. On the other hand, the RRD of technetium isotopes in the $^{16}O+^{89}Y$ system [Figs. 3(d) and 3(e)] could be reproduced by PACE2 except for the large fluctuations in the data points arising from the poor statistics of the experimental as well as Monte Carlo simulation data. This indicates the absence of ICF in the formation of technetium isotopes in this system. The mean ranges of the CF and ICF components of technetium products are shown in Table I.

The RRD of $^{92}Nb^{m}$ in the $^{16}O+^{89}Y$ system [Fig. 3(f)] shows only the ICF component. The data of the $^{12}C+^{93}Nb$ system showed very low mean ranges representative of neutron transfer products and are not shown in figures as single nucleon transfer reactions are not discussed in this paper.

The cross sections for CF and ICF in the rhodium, technetium, and niobium products are shown in Table II. It is seen from the table that the cross section for the ICF process $^{93}Nb(^{12}C,^{8}Be)^{97}Tc$ increases with the projectile energy. As we could not measure the RRD of ^{98}Rh, owing to its short half-life, it is not possible to infer about the variation of the cross section for the ICF process $^{93}Nb(^{12}C,^{4}He)^{101}Rh$. The lower limits of ICF cross sections were obtained by summing the cross sections for the observed channels, and the values are 138±14 and 180±12 mb for the ^{12}C beam of energy 63 and 77.5 MeV, respectively, and 86±9 mb for the 68 MeV ^{16}O.

DISCUSSION

The analysis of the RRD's measured in the present work shows that (i) the palladium products ($px n$ channels) are solely populated by the deexcitation of the compound nucleus formed by complete fusion of projectile and target, (ii) the rhodium products ($\alpha x n$ channels) are formed by both CF as well as ICF processes, (iii) the technetium products ($2\alpha x n$ channels) are formed only by CF in $^{16}O+^{89}Y$ and by both CF and ICF in the $^{12}C+^{93}Nb$ system at both energies of ^{12}C, and (iv) $^{92}Nb^{m}$ is found to be formed solely by the ICF process in the $^{16}O+^{89}Y$ system.

Assuming the breakup fusion model for ICF, the ejectile is expected to move undeflected at approximately beam velocity while the remaining part of the projectile will fuse with the target with an energy proportional to

TABLE II. CF and ICF[a] yields of individual evaporation residues.

	$^{12}C+^{93}Nb$				$^{16}O+^{89}Y$	
	63 MeV		77.5 MeV		68 MeV	
Nuclide	CF	ICF	CF	ICF	CF	ICF
^{99}Rh	117.3	80.2	48.9	47.5	70.4	76.2
^{96}Tc	7.3	46.4		63.1		
$^{95}Tc^{g}$	5.7	11.3	31.7	64.8		
$^{94}Tc^{g}$			8.2	5.1		
$^{92}Nb^{m}$						9.9

[a]The ICF cross section was obtained by subtracting the normalized CF component from the measured RRD.

its mass with respect to the projectile mass [14]. We generated the RRD's for the incomplete fusion products using the Monte Carlo simulation code PACE2. The following assumptions were made for the calculation.

(i) The intermediate nucleus is formed by fusion of the part of the projectile with the target with an excitation energy corresponding to the escape of the ejectile with beam velocity.

(ii) The intermediate nucleus is formed with a triangular angular momentum distribution with the maximum (l_{max}) value less than the critical angular momentum for CF by a factor equal to the mass ratio of the fusing particle to the projectile. The critical angular momenta were obtained by the method described later.

Considering that the ICF component in rhodium products arises from reactions of the type

$$^{12}C + ^{93}Nb \longrightarrow (^{8}Be + ^{93}Nb) + ^{4}He,$$
$$^{16}O + ^{89}Y \longrightarrow (^{12}C + ^{89}Y) + ^{4}He,$$

the excitation energy of the resulting compound nucleus ^{101}Rh was calculated using the simple formula [10]

$$\tfrac{2}{3}E(^{12}C)\tfrac{93}{101} + Q_{gg} \quad \text{and} \quad \tfrac{3}{4}E(^{16}O)\tfrac{89}{101} + Q_{gg}.$$

It was found to be 36 and 45 MeV for the ^{12}C+^{93}Nb system at E_{lab} = 63 and 77.5 MeV, respectively, and 34 MeV for the ^{16}O+^{89}Y system at E_{lab} = 68 MeV. The other input parameters were chosen the same way as in the case of PACE2 calculation for the CF process. Applying the same criteria of the breakup fusion model for ICF, the technetium products in ^{12}C+^{93}Nb and ^{92}Nb^{m} in the ^{16}O+^{89}Y system can be thought to be produced by the reactions

$$^{12}C + ^{93}Nb \longrightarrow (^{4}He + ^{93}Nb) + ^{8}Be,$$
$$^{16}O + ^{89}Y \longrightarrow (^{4}He + ^{89}Y) + ^{12}C.$$

The excitation energies of ^{97}Tc expected from the expression

$$\tfrac{1}{3}E(^{12}C)\tfrac{93}{97} + Q_{gg}$$

are 15 and 20 MeV at E_{lab} = 63 and 77.5 MeV, respectively. Likewise, the excitation energy of the intermediate nucleus ^{93}Nb, calculated using the expression

$$\tfrac{1}{4}E(^{16}O)\tfrac{89}{93} + Q_{gg},$$

was found to be 11 MeV. The PACE2 simulated ICF curves are shown as dotted curves in the respective figures. It may be noted that the PACE2 calculation for the RRD's of technetium products formed by ICF does not show the formation of ^{95}Tc at E_{lab} = 63 MeV and that of ^{94}Tc at E_{lab} = 77.5 MeV. The presence of ICF in ^{95}Tc at E_{lab} = 63 MeV and that of ^{94}Tc at E_{lab} = 77.5 MeV indicates that ^{97}Tc must be formed with approximate excitation energies of 24 and 36 MeV, respectively, assuming that the energy required for emission of one neutron is approximately 12 MeV.

It was found that the ICF components in the RRD's of ^{99}Rh are in reasonable agreement with the PACE2 calculations except for the slightly smaller widths of the PACE2 curves. This shows that ^{99}Rh is indeed formed by the incomplete fusion process with the projectile fragment fusing with the target with approximately same energy per nucleon. It is noteworthy here that the RRD of ^{97}Ru, measured in 77.5 MeV ^{12}C+^{93}Nb, which also contains the distribution due to the $\alpha 4n$ product, ^{97}Rh, does not show any ICF component. The absence of ICF in ^{97}Ru indicates that the excitation energy of the incompletely fused ^{101}Rh is insufficient for emission of four nucleons.

The simulated ICF curves in technetium products in ^{12}C+^{93}Nb in general agree within 20% with the deduced ICF curves in terms of the mean range. The major difference lies in the widths of the RRD's. The widths of the deduced RRD's are much higher than the corresponding PACE2 curves. The difference between the width of the simulated RRD's and those deduced by subtracting the CF part from the experimental RRD is expected as the intermediate nucleus may not be formed with a unique recoil velocity; instead, there will be a distribution of recoil velocity arising due to the kinetic energy and angular distribution of the outgoing particle. Further, the possible occurrence of multiple ICF sources which have been neglected in the PACE2 calculations can also add to the widths of calculated RRD's.

The RRD for ^{92}Nb^{m} in ^{16}O+^{89}Y could not be reproduced by the breakup fusion model in terms of both the mean range and the width. The large difference in the mean ranges may possibly be due to the contribution from the direct alpha transfer process with the outgoing fragment emitted at a grazing angle.

The RRD's of various ER's in ^{20}Ne+^{93}Nb measured by Parker, Hogan, and Asher [18] also show ICF components associated with emission of ^{16}O, ^{14}N, ^{12}C, ^{10}B, etc. Based on the breakup fusion model of the ICF process and using the experimental particle spectra, they could reproduce the RRD's of all the ER's at 106 MeV except for the technetium products. Similar modeling for the case of 148 MeV, however, could not reproduce the RRD of indium, silver, and technetium products and ^{97}Ru. They attributed the discrepancies to the contribution from direct alpha transfer and/or preequilibrium particle emission. The results of the present work also show similar trends. The RRD's of rhodium and technetium products can be reproduced reasonably well by the breakup fusion model whereas that of ^{92}Nb^{m} in ^{16}O+^{89}Y could not be reproduced.

Morgenstern *et al.* [25] suggested that the onset of ICF is governed by the relative velocity v_{rel} given by

$$v_{rel} = [2(E_{c.m.} - V_C)/\mu]^{1/2},$$

where V_C is the Coulomb barrier between projectile and target. According to this, ICF starts at v_{rel} values above $0.1c$, where c is the velocity of light. In the present study, ICF is observed even though v_{rel} is equal to $0.06c$ and $0.08c$ for 63 and 77.5 MeV ^{12}C, respectively, and $0.045c$ for 68 MeV ^{16}O. This conforms to the observation of Tserruya *et al.* [11] that ICF apparently has no threshold and it is always in competition with CF right from the Coulomb barrier. The lower value of v_{rel} for 68 MeV ^{16}O+^{89}Y may be responsible for the absence of ICF in

technetium products.

Another important question regarding the mechanism of ICF is whether it results from peripheral or central collisions. The sum rule model predicts that ICF occurs only in peripheral collisions involving $l > l_{cr}$. The experimental complete fusion cross section (σ_{CF}) is needed to extract l_{cr}. The fusion cross sections were obtained from the excitation function data measured previously [17] and using the cross sections of a few stable residues (^{102}Pd, ^{98,99}Ru) from the CASCADE code. These stable residues constitute only about 10–15 % of σ_{CF}. The σ_{CF} values thus obtained are 950±27 and 1400±37 mb for 63 and 77.5 MeV ^{12}C+^{93}Nb and 770±20 mb for 68 MeV ^{16}O+^{89}Y. The corresponding l_{cr} values are (29±1)$\hbar$, (39±1)$\hbar$, and (30±1)$\hbar$, respectively. The lower limits of the reaction cross sections (σ_R) could be obtained by adding σ_{CF} and σ_{ICF} measured in the present work. The values are 1088±33, 1580±42, and 856±22 mb for 63 and 77.5 MeV ^{12}C and 68 MeV ^{16}O beams, respectively, which correspond to the l_g values of $(31 \pm 1)\hbar$, $(42 \pm 1)\hbar$, and $(31 \pm 1)\hbar$, respectively. The angular momenta for grazing collisions (l_{gr}), calculated using the prescription of Wilczynski [26], were found to be $32\hbar$, $41\hbar$, and $30\hbar$ for the respective systems. These values are in good agreement with the l_g values obtained using the experimental σ_R, indicating that the ICF observed in the present work arises from peripheral collisions. However, more detailed experiments, particularly the measurements on gamma multiplicities in coincidence with the light ejectiles, may conclusively ascertain the angular momentum windows responsible for different ICF channels.

CONCLUSION

Recoil range distribution of ER's were studied in 63 and 77.5 MeV ^{12}C+^{93}Nb and 68 MeV ^{16}O+^{89}Y reactions. Comparison of the experimental results with the Monte Carlo simulation of RRD's following complete fusion reveal a significant contribution of ICF in the formation of rhodium and technetium products in the ^{12}C+^{93}Nb system and in rhodium and niobium products in the ^{16}O+^{89}Y system. The breakup fusion model can explain ICF in rhodium products in all three cases and that in technetium isotopes in ^{12}C+^{93}Nb at both beam energies, except for the large observed widths. The model, however, fails to explain ICF in ^{92}Nb^m in the ^{16}O+^{89}Y reaction. This may possibly be due to the contribution from direct alpha transfer from the projectile to target. The present work also shows that the probability of the occurrence of ICF in different exit channels depends on entrance channel mass asymmetry. The results corroborate the peripheral nature of the ICF process even at the projectile energy regime of 4–6 MeV/nucleon.

ACKNOWLEDGMENTS

We are grateful to Dr. R. H. Iyer, Radiochemistry Division for his encouragement and interest in this work. We are thankful to Shri D. C. Ephraim for preparing the thin metal foils. It is a pleasure to acknowledge the cooperation of operating staff of the Pelletron accelerator.

[1] C. Gerschel, Nucl. Phys. **A387**, 297c (1982).
[2] H. C. Britt and A. R. Quinton, Phys. Rev. **124**, 877 (1961).
[3] J. Galin, B. Gatty, D. Guerreau, C. Rousset, U. C. Schlotthauer-Voos, and X. Tarrago, Phys. Rev. C **9**, 1126 (1974).
[4] T. Inamura, M. Ishihara, T. Fukuda, T. Shimoda, and H. Hiruta, Phys. Lett. **68B**, 51 (1977).
[5] T. Udagawa and T. Tamura, Phys. Rev. Lett. **45**, 1311 (1980).
[6] J. Wilczynski, K. Siwek-Wilczynska, J. Van Driel, S. Gonggrijp, D. C. J. M. Hageman, R. V. F. Janssens, J. Lukasiak, R. H. Siemssen, and S. Y. Van der Werf, Nucl. Phys. **A373**, 109 (1982).
[7] J. P. Bondorf, J. N. De, G. Fai, A. O. T. Karvinen, and J. Randrup, Nucl. Phys. **A333**, 285 (1980).
[8] M. Blann, Phys. Rev. C **31**, 1285 (1985).
[9] D. J. Parker, J. J. Hogan, and J. Asher, Phys. Rev. C **39**, 2256 (1989).
[10] H. Morgenstern, W. Bohne, W. Galster, and K. Grabisch, Z. Phys. A **324**, 443 (1986).
[11] I. Tserruya, V. Steiner, Z. Fraenkel, P. Jacobs, D. G. Kovar, W. Henning, M. F. Vineyard, and B. G. Glagola, Phys. Rev. Lett. **60**, 14 (1988).
[12] H. Morgenstern, W. Bohne, W. Galster, and K. Grabisch, Phys. Rev. Lett. **52**, 1104 (1984).
[13] M. F. Vineyard, J. S. Bauer, J. F. Crum, C. H. Gosdin, R. S. Trotter, D. G. Kovar, C. Beck, D. J. Henderson, R. V. F. Jenssen, B. D. Wilkins, C. F. Maguire, J. F. Mateja, F. W. Prosser, and G. S. F. Stephens, Phys. Rev. C **45**, 1784 (1992).
[14] C. Beck, D. G. Kovar, S. J. Sanders, B. D. Wilkins, D. J. Henderson, R. V. F. Janssens, W. C. Ma, M. F. Vineyard, T. F. Wang, C. F. Maguire, F. W. Prosser, and G. Rosner, Phys. Rev. C **39**, 2202 (1989).
[15] W. Trautmann, Ole Hansen, H. Tricoire, W. Hering, R. Ritzka, and W. Trombik, Phys. Rev. Lett. **53**, 1630 (1984).
[16] H. Tricoire, C. Gerschel, N. Perrin, H. Sergolle, L. Valentin, D. Bachelier, H. Doubre, and J. Gizon, Z. Phys. A **306**, 127 (1982).
[17] B. S. Tomar, A. Goswami, A. V. R. Reddy, S. K. Das, P. P. Burte, S. B. Manohar, and Satya Prakash, Z. Phys. A **343**, 223 (1992).
[18] D. J. Parker, J. J. Hogan, and J. Asher, Phys. Rev. C **35**, 161 (1987).
[19] D. J. Parker, J. Asher, T. W. Conlon, and I. Naqib, Phys. Rev. C **30**, 143 (1984).
[20] J. Jastrzebski, H. Karwowski, M. Sadler, and P. P. Singh, Phys. Rev. C **19**, 724 (1979).
[21] H. Nifenecker, J. Blachot, J. Crancon, A. Gizon, and A. Lleres, Nucl. Phys. **A447**, 533c (1985).
[22] L. C. Northcliffe and R. F. Schilling, Nucl. Data Tables A **7**, 233 (1970).
[23] A. Gavron, Phys. Rev. C **21**, 230 (1980).
[24] P. M. Endt, At. Data Nucl. Data Tables **26**, 47 (1981).
[25] H. Morgenstern, W. Bohne, K. Grabisch, H. Lehr, and W. Stoffler, Z. Phys. A **313**, 39 (1983).
[26] J. Wilczynski, Nucl. Phys. **A216**, 386 (1973).